Downregulation of Dendritic Ih in CA1 Pyramidal Neurons after LTP

Emilie Campanac, Gaël Daoudal, Norbert Ankri, Dominique Debanne

Cellular/Molecular

Downregulation of Dendritic I_h in CA1 Pyramidal Neurons after LTP

Emilie Campanac,[1,2] Gaël Daoudal,[1,2] Norbert Ankri,[1,2] and Dominique Debanne[1,2]
[1]Inserm U641 and [2]Faculté de Médecine Nord, Université de la Méditerranée, 13916 Marseille, France

Hyperpolarization-activated (h)-channels occupy a central position in dendritic function. Although it has been demonstrated that these channels are upregulated after large depolarizations to reduce dendritic excitation, it is not clear whether they also support other forms of long-term plasticity. We show here that nearly maximal long-term potentiation (LTP) induced by theta-burst pairing produced upregulation in h-channel activity in CA1 pyramidal neurons. In contrast, moderate LTP induced by spike-timing-dependent plasticity or high-frequency stimulation (HFS) downregulated the h-current (I_h) in the dendrites. After HFS-induced LTP, the h-conductance (G_h) was reduced without changing its activation. Pharmacological blockade of I_h had no effect on LTP induction, but occluded EPSP-to-spike potentiation, an input-specific facilitation of dendritic integration. Dynamic-clamp reduction of G_h locally in the dendrite mimicked the effects of HFS and enhanced synaptic integration in an input-selective way. We conclude that dendritic I_h is locally downregulated after induction of nonmaximal LTP, thus facilitating integration of the potentiated input.

Key words: **EPSP–spike plasticity; homeostatic plasticity; dendrite; dendritic integration; dynamic clamp; Hebbian**

Introduction

In CA1 pyramidal neurons, EPSP waveform is regulated by several voltage-gated currents located in the dendrite and the soma (Andersen, 1990; Reyes, 2001; Spruston, 2008). Among them, the hyperpolarization-activated cationic current (I_h) attenuates EPSP amplitude and reduces neuronal excitability (Maccaferri et al., 1993; Gasparini and DiFrancesco, 1997; Magee, 1998; Poolos et al., 2002). The h-current is prominent in the dendrites of CA1 neurons (Magee, 1998; Lörincz et al., 2002) and can be regulated by neuronal activity. Homeostatic (i.e., compensatory) upregulation of I_h is induced in CA1 neurons by hyperthermia (Chen et al., 2001), postsynaptic depolarization (van Welie et al., 2004), or induction of large long-term potentiation (LTP) with theta-burst pairing (TBP) (Fan et al., 2005). These regulations limit postsynaptic excitation. However, it is not yet clear whether h-channels also support nonhomeostatic (i.e., Hebbian-like) plasticity to enhance intrinsic excitability (IE).

Integration of synaptic inputs to produce an action potential (AP) is a fundamental step in the transfer of the neuronal message, because spiking activity represents the main neuronal output (Andersen, 1990; Spruston et al., 1994). Synaptic integration is relatively well characterized, but its dynamics remain poorly understood. In the hippocampus, LTP of excitatory synaptic transmission is induced by brief high-frequency stimulation (HFS) (100 Hz) of afferent fibers (Bliss and Lømo, 1973). In parallel, the postsynaptic firing probability in response to a given input is enhanced (Bliss et al., 1973; Andersen et al., 1980; Abraham et al., 1987). This second component has been called EPSP-to-spike potentiation (E-S potentiation), which is synergistic to LTP and functionally important (Daoudal and Debanne, 2003; Hanse, 2008). E-S potentiation is not entirely abolished by $GABA_A$ and $GABA_B$ receptor antagonists (Hess and Gustafsson, 1990; Asztely and Gustafsson, 1994; Daoudal et al., 2002; Marder and Buonomano, 2003; Staff and Spruston, 2003), indicating that it may involve the long-lasting modulation of intrinsic voltage-gated conductances. GABA receptor-independent E-S potentiation is input specific (Hess and Gustafsson, 1990; Daoudal et al., 2002; Campanac and Debanne, 2008), suggesting that the underlying changes in IE might be restricted to a small dendritic region. We show here for the first time that E-S potentiation that follows induction of moderate LTP in CA1 neurons is attributable to Hebbian long-lasting downregulation of dendritic I_h.

Materials and Methods

Slice preparation and electrophysiology. Hippocampal slices were obtained from 15- to 27-d-old rats according to institutional guidelines for the care and use of laboratory animals (Directive 86/609/EEC and French National Research Council). Slices (350 μm) were cut in a solution (in mM: 280 sucrose, 26 $NaHCO_3$, 10 D-glucose, 1.3 KCl, 1 $CaCl_2$, and 10 $MgCl_2$) and were maintained for 1 h at room temperature in oxygenated (95% O_2/5% CO_2) artificial CSF (ACSF; in mM: 125 NaCl, 2.5 KCl, 0.8 NaH_2PO_4, 26 $NaHCO_3$, 3 $CaCl_2$, 2 $MgCl_2$, and 10 D-glucose). Each slice was transferred to a temperature-controlled (29°C) chamber with oxygenated ACSF. $GABA_A$ channels were blocked with picrotoxin (PiTX) and the CA1 area was surgically isolated.

Field potentials were recorded using glass microelectrodes filled with 3

Received April 3, 2008; revised July 7, 2008; accepted July 21, 2008.

This work was supported by Inserm Avenir (D.D.); Centre National de la Recherche Scientifique, Agence Nationale de la Recherche (Neurosciences, neurologie et psychiatrie); Fondation pour la Recherche Médicale doctoral grants (E.C., G.D.); and Ministry of Research doctoral grants (E.C., G.D.) and Action Concertée Incitative Jeunes Chercheurs (D.D.). We thank L. Fronzaroli-Molinieres for excellent technical assistance, T. V. P. Bliss, B. H. Gähwiler, J. M. Goaillard, and M. Seagar for constructive comments on this manuscript, and O. Caillard, I. L. Kopysova, and R. H. Cudmore for helpful discussion.

Correspondence should be addressed to Dominique Debanne at the above address. E-mail: dominique.debanne@univmed.fr.

DOI:10.1523/JNEUROSCI.1411-08.2008

 0270-6474/08/288635-09$15.00/0

M NaCl. For whole-cell recordings from CA1 pyramidal neurons, electrodes were filled with a solution containing the following (in mM): 120 K-gluconate, 20 KCl, 10 HEPES, 0.5 EGTA, 2 $MgCl_26H_2O$, and 2 Na_2ATP. Stimulating pipettes were filled with extracellular saline. LTP was induced with three protocols. In most experiments, LTP was induced with 10 bursts of 10 shocks at 100 Hz (HFS). The bursts were delivered at 0.3 Hz. In this case, the averaged number of spikes triggered by the summated EPSPs was 46 ± 4 ($n = 17$). LTP was also induced by pairing subthreshold synaptic stimulation with backpropagated APs (bAPs) at theta frequency (5 Hz; TBP). Here, three trains of 10 bursts were repeated at 0.1 Hz, with each burst composed of five EPSPs paired with five bAPs (delay, +5 ms) at 100 Hz. Here, the number of postsynaptic spikes during TBP was 150. Finally, LTP was also induced by pairing single EPSPs with single bAPs at 0.33 Hz [spike-timing-dependent plasticity (STDP); delay, +5/+50 ms; 100 repetitions] (Debanne et al., 1998; Campanac and Debanne, 2008). Drugs were bath applied. PiTX was purchased from Sigma, and [4-(*N*-ethyl-*N*-phenylamino)-1,2-dimethyl-6-(methylamino) pyrimidinium chloride] (ZD-7288) and D-AP5 were purchased from Tocris Bioscience.

Data acquisition and analysis. Recordings were obtained using an Axoclamp-2B amplifier and Acquis1 and pClamp8 software. Data were analyzed with IGOR Pro. Only perfectly stable recordings were included in final analysis. Recordings were rejected when bridge balance varied >10%. Pooled data are presented as mean ± SE.

Characterization of I_h was assessed in the presence of TTX (500 nM), PiTX (100 μM), kynurenate (2 mM), Ni^{2+} (200 μM), TEA (5 mM), and 4-AP (100 μM). Subtraction of control records from those obtained after ZD-7288 (in this particular case, 50 μM) application allowed isolation of I_h. Activation was assessed by voltage steps from a potential of −50 to −60/−120 mV. Deactivation was analyzed in tail currents evoked by stepping from −75 to −70/−45 mV. All currents were fitted with monoexponential functions. Activation and deactivation time constants were averaged and plotted. Reversal potential (E_h) was determined by linear extrapolation of the tail-current amplitude (−37.7 ± 0.9 mV; $n = 3$).

Model of G_h. A model of G_h using the Hodgkin-Huxley formalism was developed. Equations describing the voltage dependence of G_h were based on a deterministic Hodgkin-Huxley model with one variable (n, the gating particle for activation), which obeys first-order kinetics. The h-current was given by $I_h = G_h(V_m - E_h)$, where V_m is the membrane potential, $E_h = -37.7$ mV, and the h-conductance $G_h = G_{hmax}n$. The activation and deactivation time constants were determined by fitting experimental data (see above).

The differential equation $dn(V,t)/dt = \alpha(V)[1 - n(V,t)] - \beta(V)n(V,t)$ was solved. This equation corresponds to $d(V,t)/dt = [n_\infty(V) - n(V,t)]/\tau(V)$ with the steady-state activation parameter as $n_\infty(V) = \alpha_n(V)/[\alpha_n(V) + \beta_n(V)]$, and the activation time constant $\tau(V) = 1$ for $V > -30$ mV; otherwise, $\tau(V) = 1/[\alpha_n(V) + \beta_n(V)]$ with $\alpha_n = 0.0204/(1 + \exp[(V + 98.68)/13.24])$ and $\beta_n = 0.0176/(1 + \exp[-(V + 57.96)/13.2])$.

Dynamic clamp. To add or subtract G_h in dendrites, a dynamic-clamp system was developed (Prinz et al., 2004). The system of dynamic clamp consisted of an embedded processor with real-time operating system that was programmed and controlled from a host PC computer with the graphical language LabView 7-Express containing the LabView Real-Time module (Carlier et al., 2006). The feedback loop ($F = 38$ kHz) continuously read the membrane potential V_m from the Axoclamp-2B, computed G_h, and generated an output, I_h, according to the following equation: $I_h = G_h(V_m - E_h)$. A reconfigurable input/output (I/O) module (NI PXI-7831R) allowed monitoring of V_m and generation of I_h. The access speed of analog–digital and digital–analog conversions on the input/output module was optimized by a field-programmable gate array.

To minimize calculations during the calculation loop, specific arrays of $\tau(V)$ and $n_\infty(V)$ were initialized with a resolution of 0.1 mV. For a given voltage, corresponding values of $\tau(V)$ and $n_\infty(V)$ were obtained by linear interpolation from the array. The numerical integration, based on Euler's method, involved a simple linear extrapolation of the gating variable given by the following equation: $n_{k+1} = n_k + (n_\infty - n_k)dt$.

An Axoclamp-2B amplifier (Molecular Devices) was used for dynamic-clamp experiments, and the bridge balance was monitored continuously to minimize series resistance artifacts. Only recordings with series resistance <25 MΩ were kept for further analysis.

The model was validated with addition and subtraction of the h-conductance. Families of voltage traces evoked by depolarizing and hyperpolarizing pulses of current (+50/−50 pA) were recorded in controls. Compared with a previous study (Magee, 1998), activation and inactivation time constants were slightly slower. This small difference is attributable to the age dependence of the kinetics of I_h (Vasilyev and Barish, 2002). In the presence of 5 mM Cs^+ in the external saline, the input resistance increased and the depolarizing sag was suppressed. The addition of the simulated h-conductance with the dynamic clamp (range, 5–7 nS; $n = 3$) decreased the input resistance and restored the sag. In fact, voltage signals recorded in these conditions ($Cs^+ + I_h$ Dyn) were virtually identical to the control traces. Conversely, the injection of an anti-h-conductance increased the input resistance and suppressed the sag. An external digital device [microcontroller PIC-16F876A (Microchip)] was used to facilitate the adjustment of the values of G_h during the experiment. Thus, digitized values of this variable were directly read in real time by the I/O module.

The model of G_h was designed with current traces recorded from the soma, but the conductance was injected in the dendrite. This procedure is justified because the dendritic site of current injection was rather proximal in these experiments (~70 μm), and somatic and dendritic I_h display rather similar activation and deactivation kinetics (Magee, 1998). The consequence of poor space clamp of the dendrites during the measurement of I_h in the soma was minimized because small voltage deflections were used in our dynamic-clamp experiments. In fact, modeling studies indicate that significant errors occur in the dendrite for voltage commands >30 mV (Day et al., 2005). Importantly, hyperpolarizing pulses did not exceed 20 mV, and EPSPs remained relatively small (~10 mV) in our experiments.

Results

Regulation of I_h depends on LTP amplitude

All experiments were performed in the presence of the $GABA_AR$ channel blocker PiTX (100 μM). EPSPs were evoked in CA1 pyramidal neurons recorded in whole-cell configuration by stimulation of the Schaffer collaterals (SCs) at 70–120 μm from the pyramidal cell layer. Apparent input resistance (R_{in}) measured with large pulses to recruit I_h (100–150 pA, 0.8–1 s) was found to depend on LTP amplitude. In agreement with a previous study (Fan et al., 2005), large LTP (>250%) induced by TBP was associated with a decrease in apparent R_{in} (significant [Mann–Whitney (MW), $p < 0.01$] decrease in 4/5 cases) (Fig. 1*A*). In contrast, moderate LTP (<150%) induced by TBP was associated with an increase in apparent R_{in} (significant increase in 4/4 cases) (Fig. 1*B*), suggesting a reduction in I_h. Physiologically, this latter regulation is important because *in vivo*, hippocampal LTP is also in the 120–150% range (Abraham et al., 2002). Changes in apparent R_{in} were also analyzed for HFS- and STDP-induced LTP, which are associated with E-S potentiation (Daoudal et al., 2002; Campanac and Debanne, 2008). When the data obtained with the three LTP protocols were pooled together, a significant correlation between apparent R_{in} and LTP amplitude was found (Fig. 1*C*). HFS and STDP protocols led to moderate LTP (mean, 154 and 123%, respectively) and were associated with increased apparent R_{in} (HFS, significant increase in 8/14 cells; STDP, significant increase in 7/13 cells). On average, moderate LTP (<150%) induced by these protocols increased apparent R_{in} to 109 ± 2% ($n = 12$) and 108 ± 3% ($n = 11$), respectively. Thus, I_h is downregulated for small LTP amplitudes.

If this hypothesis is true, E-S potentiation should be preferentially observed for moderate LTP. Consistent with this idea, E-S potentiation induced by HFS was maximal for modest LTP (<150%) but declined and reversed when LTP was larger than 160% (MW test, $p < 0.05$) (Fig. 1*D*). The downregulation of I_h

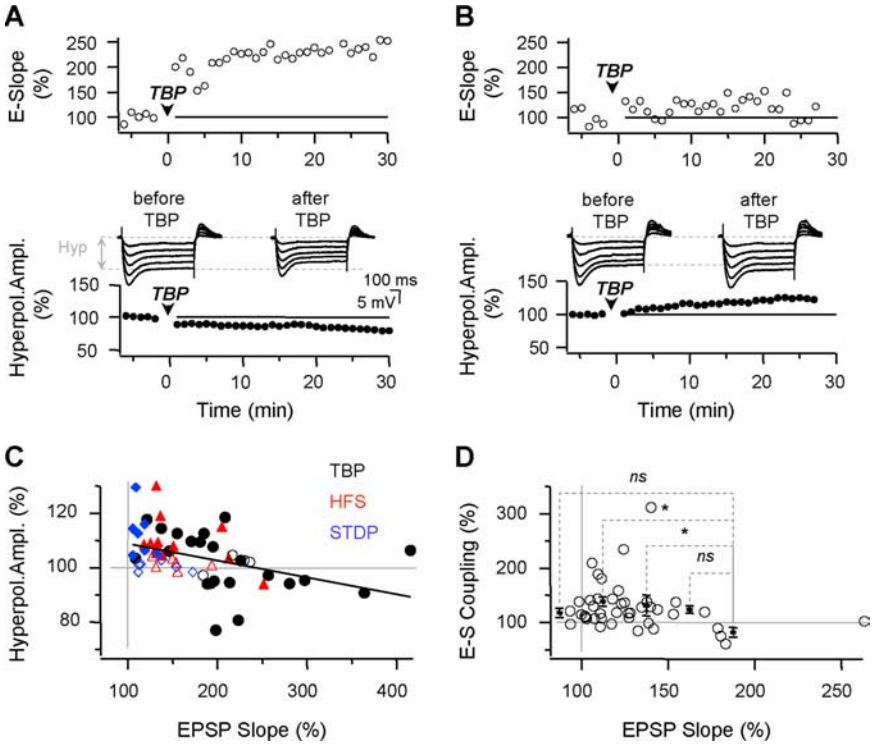

Figure 1. Regulation of I_h depends on LTP magnitude. ***A***, Large TBP-induced LTP (225%) is accompanied by an increase in I_h. Top graph, Time course of LTP. Bottom graph, Time course of the apparent R_{in} measured with a large hyperpolarizing pulse of current (−100 pA, 1 s). Middle traces, Family of voltage deflections measured at constant V_m in response to a series of current pulses (−20/−100 pA) before and 30 min after TBP. ***B***, Moderate TBP-induced LTP (125%) is associated with a decrease in h-channel activity. Note the increase in the amplitude of the hyperpolarization after TBP (middle traces and bottom plot). ***C***, Normalized hyperpolarization amplitude versus normalized EPSP slope for TBP, STDP, and HFS (open symbols, not significant changes). A significant linear anticorrelation was observed ($y = -0.062x + 115$; $r = 0.41$; $p < 0.005$). ***D***, E-S potentiation depends on the magnitude of LTP. Normalized E-S changes as a function of synaptic potentiation are shown. Note that maximal E-S potentiation is obtained for moderate potentiation (120–140%), whereas E-S depression is consistently observed for maximal potentiation (>160%). Black squares, Mean changes in E-S coupling calculated in classes of 25%. Asterisks indicate statistically significant differences (Mann–Whitney *U* test, $p < 0.05$). Hyperpol. Ampl., Hyperpolarization amplitude.

associated with moderate LTP has not yet been described. Because it was consistently observed with HFS, all subsequent experiments were performed with this protocol.

HFS downregulates I_h

Increase in apparent R_{in} was associated with the reduction in the sag amplitude (−0.6 ± 0.3 mV; $n = 12$) (Fig. 2*A*), indicating that I_h was downregulated. These effects were stimulus dependent because apparent R_{in} and sag amplitude were not affected in the absence of HFS (102 ± 3% and 0.0 ± 0.1 mV; $n = 6$, respectively). In the presence of 50 μM D-AP5, HFS produced no change in EPSP slope (100 ± 4%; $n = 11$), apparent R_{in} (103 ± 2%), or sag amplitude (0.1 ± 0.2 mV) (Fig. 2*A*), indicating that I_h reduction requires NMDA receptor (NMDAR) activation. I_h contributes to resting membrane potential (RMP) because a small fraction of h-channels is open at rest (Maccaferri et al., 1993; Gasparini and DiFrancesco, 1997; Magee, 1998). We therefore tested whether RMP at the soma was changed after HFS. In fact, RMP remained constant (−0.0 ± 0.2 mV; $n = 12$) (Fig. 2*A*), suggesting that the downregulation of I_h might be spatially restricted within a small dendritic region and therefore too small to influence RMP at the soma. To distinguish between a reduction in G_h and a leftward shift in its activation curve, I_h was studied in voltage clamp before and after LTP induction (128 ± 3%; $n = 9$). No apparent shift in activation was noted (half activation, −77.4 mV vs −75.9 mV after HFS; MW, $p > 0.05$), but a significant reduction in G_h was observed after LTP induction (87 ± 4%; $n = 9$; MW, $p < 0.001$) (Fig. 2*B*).

Because h-channels are located in the dendrites, maximal change may occur there. To test this hypothesis, dual whole-cell soma and dendrite recordings (average distance, 66 μm) were obtained from CA1 neurons (Fig. 3*A*). HFS produced a significantly larger effect when the current pulse was injected in the dendrite (108 ± 4 vs 120 ± 4% in the dendrite; $n = 4$; paired *t* test, $p < 0.05$) (Fig. 3*B*). Consistent with a local change in I_h, HFS produced a larger hyperpolarization in the dendrite (−0.9 ± 0.4 mV vs −1.5 ± 0.3 mV in the dendrite; $n = 4$; paired *t* test, $p < 0.05$). Apparent R_{in} measured in the dendrite and LTP were inversely correlated (Fig. 3*C*), thus confirming our preceding observations.

I_h blockade abolishes E-S potentiation

HFS of the SCs persistently enhanced both synaptic transmission (126 ± 4% of the control EPSP slope; $n = 24$) and E-S coupling (135 ± 10% of the control; $n = 24$) (Fig. 4*A*) recorded extracellularly in the pyramidal cell layer (Daoudal et al., 2002). To determine the role of I_h in the expression of E-S potentiation, HFS was applied after the pharmacological blockade of h-channels with external Cs^+ (2.5 mM) or ZD-7288 (1 μM). In these conditions, HFS induced LTP [respectively, 189 ± 6% ($n = 7$) and 135 ± 4% ($n = 8$)], but E-S potentiation was never observed [respectively, 96 ± 4% ($n = 7$) and 101 ± 10% ($n = 8$)] (Fig. 4*B*,*C*). Our results therefore indicate that pharmacological blockade of I_h prevents the expression of E-S potentiation but not LTP.

Changes in EPSP waveform

If I_h is downregulated in the dendrites, EPSP waveform should be prolonged after LTP induction. Field EPSPs (fEPSPs) were recorded in the stratum radiatum, and stimulus intensity was adjusted before and after LTP to collect families of fEPSP slopes. fEPSPs with matching slopes displayed slightly prolonged decays after LTP. On average, the fEPSP integral increased to 108 ± 2% ($n = 7$; MW, $p < 0.001$). Similar observations were made in single CA1 pyramidal neurons (116 ± 5% of the EPSP integral; $n = 8$). We then determined whether similar modifications were also induced by pharmacological blockade of I_h. Application of external Cs^+ or ZD-7288 increased the integral of matching-slopes EPSPs both in field potential (113 ± 2%; $n = 6$; MW, $p < 0.01$) and whole-cell recordings (129 ± 6%; $n = 7$). Thus, HFS-induced changes in EPSP waveform could be mimicked by blocking h-channels.

H-channels determine synaptic integration

Next, we tested whether the blockade of I_h mimicked the effects of HFS, i.e., increased apparent R_{in} and reduced sag and E-S potentiation, but no change in RMP. Blocking I_h with external Cs^+ did

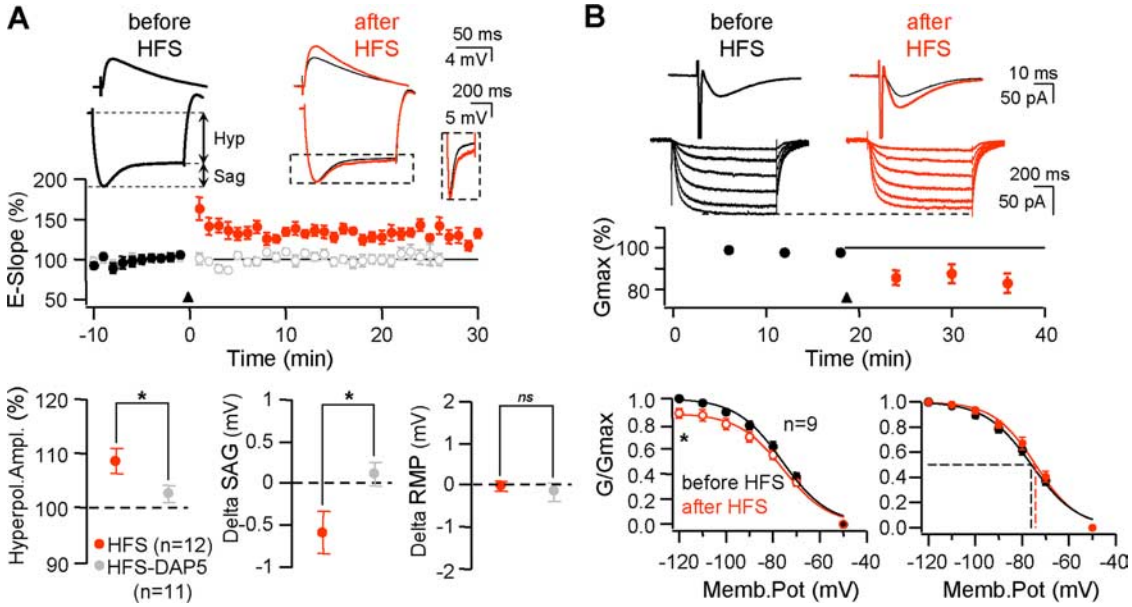

Figure 2. Long-lasting decrease in I_h after HFS. ***A***, Current-clamp analysis. Top, Time course of LTP in control (red) or in the presence of D-AP5 (gray). Top traces, EPSPs and representative voltage traces evoked by large hyperpolarizing pulses of current (−100/−150 pA, 0.8–1 s), before and after LTP. HFS induced LTP and enhanced the apparent R_{in} [superimposed traces, before (black) and after (red) HFS]. Bottom, Summary of changes in apparent R_{in} (left), depolarizing sag (middle), and RMP (right) (*$p < 0.05$; ns, $p > 0.05$). ***B***, Voltage-clamp analysis. Top, Time course of the maximal conductance G_h. Representative traces showing EPSC potentiation (top traces) and reduction in I_h (bottom traces) are shown. Bottom, Normalized conductance–voltage relations before (black circles) or after (red circles) HFS. Bottom right, Filled red circles correspond to data normalized to the current evoked by a voltage step to −120 mV. Amplitudes of the h-current were measured at 800 ms. Values of G_h were fitted with Boltzmann functions. Hyp, Hyperpolarization; Hyperpol. Ampl., hyperpolarization amplitude; Memb. Pot, membrane potential.

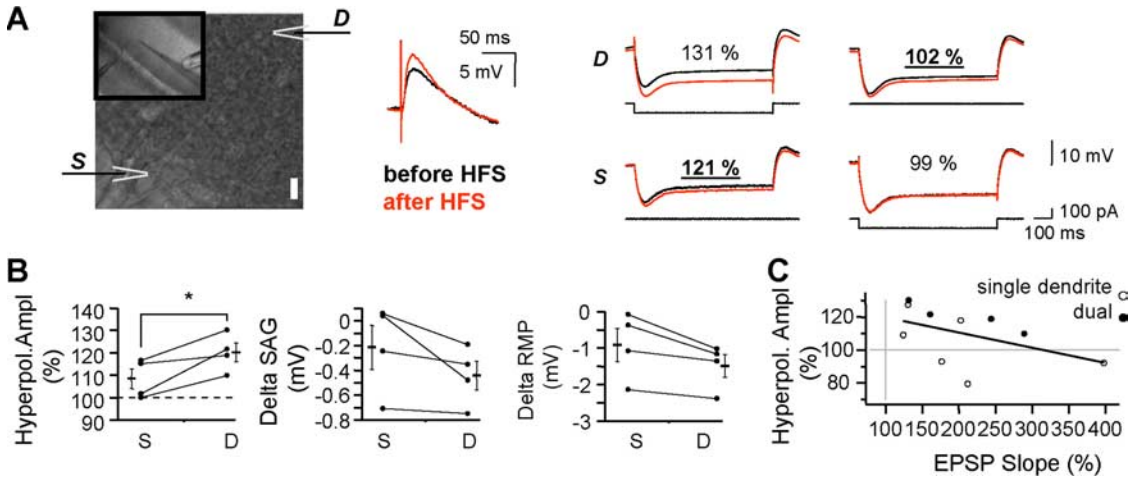

Figure 3. Local increase in apparent R_{in} in the dendrite after LTP induction. ***A***, Left, Position of recording and stimulating pipettes (inset) on the soma (S) and the dendrite (D) of a CA1 pyramidal neuron. Scale bar, 10 μm. Middle, Superimposed EPSPs before and after HFS recorded in the soma. Right, Voltage responses to hyperpolarizing current pulses injected in the dendrite (top) or the soma (bottom), before (black), and after (red) LTP induction. Note the increased apparent R_{in} when current is injected in the dendrite. To minimize bridge errors, voltage deflections measured with the electrode that did not inject current were normalized, and these values (underlined) were retained for further analysis. ***B***, Left, Normalized hyperpolarization amplitude measured when the current is injected in the soma and the dendrite. Middle, Changes in sag amplitude. Right, Change in RMP. ***C***, Plot of apparent R_{in} versus the EPSP slope. Note the correlation ($y = -0.092x + 129.08$; $r = 0.47$). Hyperpol. Ampl., Hyperpolarization amplitude. *$p < 0.05$.

not affect fEPSP slope (103 ± 5%; $n = 5$) but significantly reduced E-S coupling (79 ± 5%; $n = 5$). To further understand the underlying mechanisms, CA1 neurons were whole-cell recorded. Bath application of external Cs^+ (2.5 mM) or ZD-7288 (1 μM) reduced E-S coupling measured in CA1 neurons (27 ± 7%; $n = 9$) (Fig. 5*A*), because the hyperpolarization (−6.0 ± 1.5 mV; $n = 9$) prevented spiking evoked by EPSPs. After compensation of the hyperpolarization, Cs^+/ZD-7288 dramatically enhanced E-S coupling (255 ± 50%; $n = 6$) (Fig. 5*B*). H-channels do not control E-S coupling through spike-threshold modulation, because the AP threshold (defined as V_m, where $dV/dt > 10$ mV/ms) was unchanged in the presence of ZD or Cs^+ (change, −0.3 ± 0.6 mV; $n = 6$; paired t test, $p > 0.05$). In conclusion, two opposite effects on E-S coupling are induced by h-channel blockers: (1) a hyperpolarization-induced E-S depression and (2) an E-S potentiation caused by the suppression of EPSP attenuation.

The fact that the sag was totally abolished, the RMP strongly hyperpolarized, and the apparent R_{in} increased by 162 ± 11% indicates that a global reduction in I_h is not appropriate to reproduce the HFS-induced effects. Next, we applied external Cs^+ with a patch pipette to downregulate h-channel activity locally in the dendrites (Fig. 5*C*). In these conditions, apparent R_{in} was

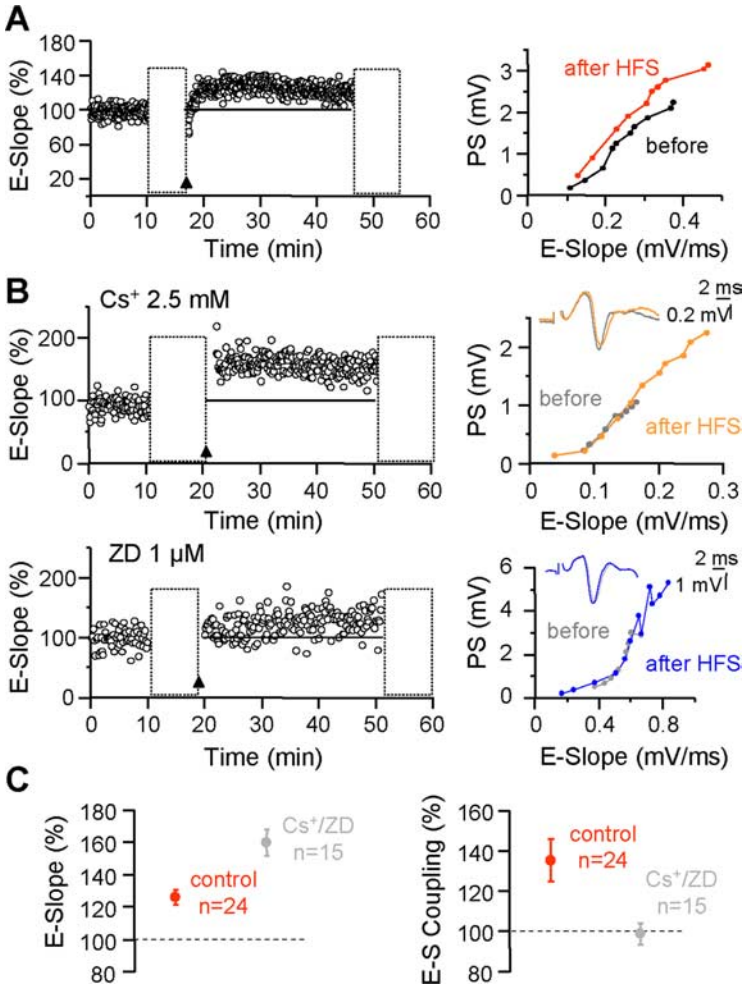

Figure 4. Occlusion of E-S potentiation by I_h blockers. ***A***, LTP (left) and E-S potentiation (right) induced by HFS (100 Hz; black triangle) in a representative slice. Dashed areas correspond to the test of E-S coupling. Right, Population spike (PS) amplitude as a function of EPSP slope before and after HFS. ***B***, I_h blockers prevented induction of E-S potentiation but not LTP. E-S curves before (gray) and after LTP in the presence of Cs^+ or ZD-7288 are shown. ***C***, Summary of normalized EPSP slope (left) and E-S changes (right) after HFS.

increased (109 ± 2%; $n = 6$; MW, $p < 0.001$) without significantly changing RMP (−1.0 ± 0.3 mV; $n = 6$). This effect was specific because no change in the apparent R_{in} (100 ± 1%; $n = 6$) was observed when external saline was applied. Because local positive pressure depresses synaptic transmission (Fagni et al., 1987), we used dynamic clamp to reduce electronically G_h in the dendrite and determine integration of evoked EPSPs.

Local downregulation of I_h with fast dynamic clamp mimics E-S potentiation

A model of G_h was developed using the Hodgkin-Huxley formalism (for details, see Materials and Methods) (Fig. 6*A–C*). The model was validated with the dynamic-clamp technique by comparing the addition or subtraction of G_h with the action of pharmacological blockade of h-channels. Addition of the h-conductance restored the electrical phenotype of the neuron when h-channels were blocked pharmacologically (Fig. 6*D*). Conversely, subtraction of G_h mimicked the pharmacological blockade of h-channels (Fig. 6*E*). Dual whole-cell soma and dendrite recordings (mean distance, 60 ± 12 µm) were obtained, and EPSPs were evoked by stimulating the SCs at the same dendritic location. The dendritic pipette was linked to a dynamic-clamp device allowing injection of an anti-G_h in the dendrite (Fig. 7*A*). After monitoring the integration properties of the neuron in control conditions, the anti-G_h was injected in the dendrite to mimic the HFS-induced effects on dendritic integration. The magnitude of anti-G_h (−1/−2.5 nS) was adjusted to produce a 10–15% increase in apparent R_{in} tested with a hyperpolarizing current pulse (1 s, 150 pA) (Fig. 7*A*) in the somatic recording (113 ± 1%; $n = 5$). In fact, the other characteristics were virtually identical to those observed after LTP induction. The sag measured at the soma was reduced (−0.3 ± 0.1 mV; $n = 5$), but RMP remained constant (0 ± 0 mV; $n = 5$) after dendritic anti-G_h injection. Most importantly, E-S coupling was enhanced (139 ± 12%; $n = 5$) (Fig. 7*B*,*C*). Thus, these results demonstrate that reduction of the dendritic G_h facilitates integration without affecting RMP at the soma.

Input specificity of the change in dendritic integration

E-S potentiation is input specific (Daoudal et al., 2002; Campanac and Debanne, 2008). Therefore, we examined whether the enhanced integration produced by a reduction of the dendritic G_h was also input specific. A second synaptic pathway (St2) was stimulated in the proximal apical dendrite (~20–40 µm from the cell-body layer) (Fig. 7*D*). When G_h was reduced in the dendrite, the EPSP integral was differentially increased in the distal input (125 ± 10% of the EPSP integral on St1 vs 113 ± 7% for St2; $n = 4$; paired t test, $p < 0.05$) (Fig. 7*E*), further supporting the input specificity of E-S potentiation. Together, these data confirm that the downregulation of G_h in the dendrite accounts for the input-specific E-S potentiation observed after LTP induction (Hess and Gustafsson, 1990; Daoudal et al., 2002; Campanac and Debanne, 2008).

Discussion

We show here that the persistent downregulation of I_h represents a major mechanism for the expression of long-term enhancement of synaptic integration in CA1 neurons. This finding is physiologically important because moderate LTP (120–150%) is mostly observed *in vivo* (Abraham et al., 2002). The electrophysiological signatures of I_h were decreased after induction of moderate LTP. The apparent R_{in} measured with large hyperpolarizing pulses was increased, and the depolarizing sag was reduced. These effects were more prominent in dendritic recordings. In addition, the blockade of I_h with external Cs^+ or ZD-7288 prevented induction of E-S potentiation but not LTP. Moreover, the modification in the EPSP waveform associated with LTP could be mimicked by pharmacological blockade of I_h. Finally, the reduction of dendritic G_h by local application of external Cs^+ or by the injection of an anti-G_h with the dynamic-clamp technique reproduced the modifications induced by HFS and enhanced integration.

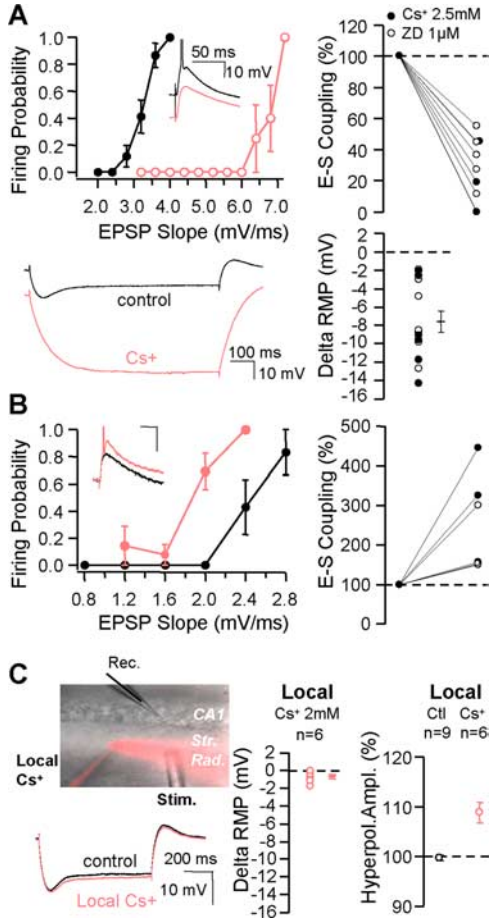

Figure 5. Control of E-S coupling by h-channels. ***A***, h-Channel blockade hyperpolarized the neuron and depressed E-S coupling. Top, Bath application of Cs^+ (2.5 mM) or ZD-7288 (1 μM) depressed E-S coupling (top left) and hyperpolarized the neuron (bottom left). Right, Summary of the effect of Cs^+ and ZD-7288 on E-S coupling ($n = 9$) and on the resting membrane potential. ***B***, h-Channel blockade enhanced E-S coupling at constant potential. When the potential at the cell body was kept constant with DC current injection, Cs^+ or ZD-7288 enhanced the E-S coupling ($n = 6$). ***C***, Local perfusion of Cs^+ was able to decrease I_h without affecting the RMP measured at the soma. Left, Cs^+ application was visualized with Alexa568 (100 μM). The pipette filled with Cs-Alexa was positioned on the surface of the slice at 60–100 μm from the soma, and the diameter of the Cs-Alexa stream was estimated to be ~60–70 μm. Right, Changes in RMP and in apparent input resistance. The amplitude of the sag was decreased by -0.3 ± 0.1 mV ($n = 6$). No change in the amplitude of the hyperpolarization (Hyperpol. Ampl.) was observed when the external saline was applied. Rec., Recording electrode; Str. Rad., stratum radiatum.

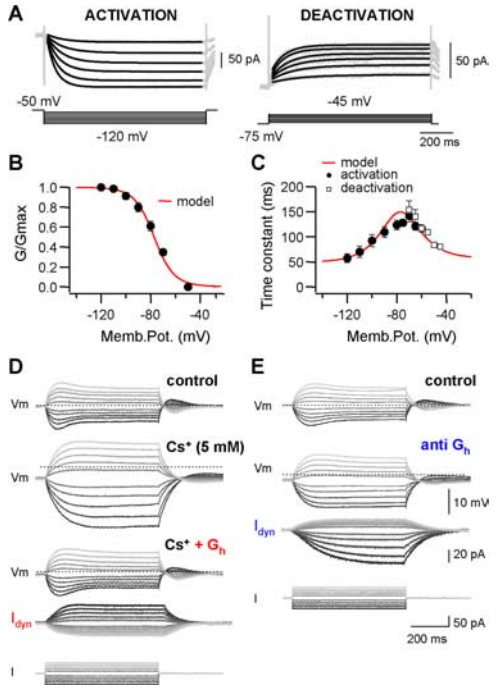

Figure 6. Characterization of I_h in CA1 pyramidal neurons and modeling. ***A***, Currents were isolated after subtracting control currents from those generated in the presence of ZD-7288 (see Materials and Methods). Left, h-Channels were activated by holding the cell at −50 mV and stepping to −120 mV with 10 mV increments. Currents generated were well fitted with a monoexponential function (black lines). Right, Deactivation of h-channels was studied in neurons held at −75 mV by stepping to −45 mV with 5 mV increments. The data were also well fitted with a monoexponential function. ***B***, Normalized conductance–voltage (G–V) relation was estimated from the currents shown in ***A***. The modeled activation curve is represented in red. ***C***, The mean activation (filled circles) and deactivation (open squares) time constants plotted against the membrane potential. ***D***, ***E***, Validation of the model with the fast dynamic-clamp technique. CA1 pyramidal cells were recorded in the whole-cell configuration. Families of voltage traces evoked by depolarizing and hyperpolarizing pulses of current (+50/−50 pA) were recorded in different conditions: control (top) and in the presence of Cs^+ (***D***, middle), Cs^+ and dynamic G_h (***D***, bottom), or dynamic anti-G_h (***E***, bottom). The respective families of dynamic currents are illustrated below (I_{dyn}). Memb. Pot., Membrane potential.

Thus, the downregulation of I_h activity produced a Hebbian-like form of intrinsic plasticity because elevated synaptic activity is associated with facilitation in postsynaptic spiking.

Hebbian and homeostatic regulation of I_h

Hebbian and homeostatic plasticity are functionally opposed, but they are thought to coexist to stabilize neuronal activity in brain circuits (Turrigiano and Nelson, 2004). Experimental evidence bridging the two types of plasticity was, however, missing (Debanne et al., 2003; Zhang and Linden, 2003). Our results indicate that I_h expressed in CA1 pyramidal cell dendrites may undergo Hebbian and homeostatic plasticity in a single physiological context. Whereas very large LTP is associated with the upregulation of h-channel activity as previously observed (Fan et al., 2005), modest synaptic potentiation is accompanied by a decrease in I_h. The downregulation observed for small LTP was confirmed with two other LTP induction protocols (STDP and HFS), and apparent R_{in} and LTP amplitude were inversely correlated. The switch from Hebbian to homeostatic plasticity is further supported by the fact that E-S potentiation was maximal for mild LTP, whereas E-S depression was consistently observed for very large LTP. The transition from Hebbian to homeostatic plasticity probably results from the different levels of postsynaptic depolarization attained in the dendrites during conditioning. In fact, the number of postsynaptic spikes was much higher with the protocol (TBP) that produced the higher proportion of homeostatic changes (150 vs ~46 for HFS). Thus, two opposite forms of intrinsic plasticity (i.e., Hebbian and homeostatic) coexist in CA1 neurons to stabilize the neuronal excitability in a physiological range.

Activity-dependent downregulation of h-channel activity

All the hallmarks of I_h were affected after induction of LTP. Apparent R_{in} tested with large current steps was enhanced, the depolarizing sag was diminished, and G_h was reduced by ~15% without affecting its activation curve. In addition, we show that blocking I_h with external Cs^+ or ZD-7288 prevented E-S potentiation without reducing LTP magnitude. The slight increase in LTP in the presence of I_h blockers was probably caused by enhanced EPSP summation during HFS, thus optimizing NMDAR activation. ZD-7288 has been shown to have presynaptic effects at concentrations >10 μM but not at the concentration used here (1

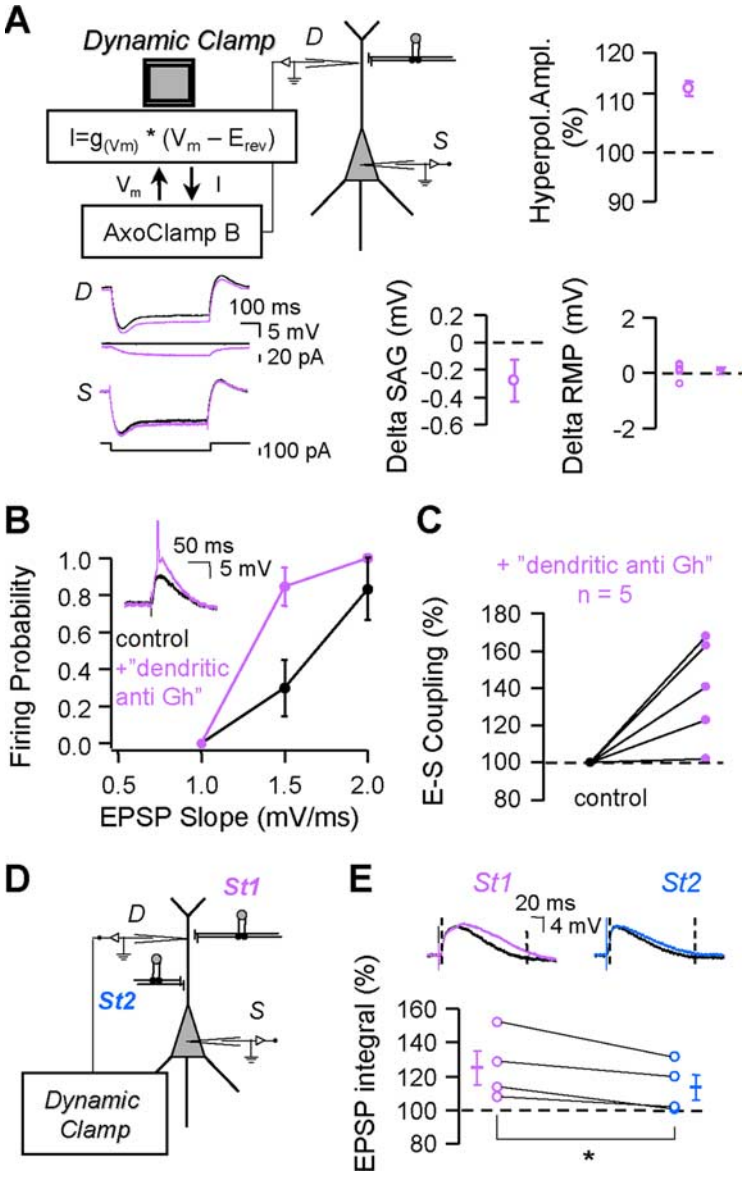

Figure 7. Dynamic-clamp reduction of dendritic G_h mimics E-S potentiation. ***A***, Top left, Recording configuration: dual soma–dendrite whole-cell recording. The anti-G_h was injected through the dendritic electrode (D), whereas E-S coupling was evaluated with the somatic electrode (S). Bottom left, Control (black) and anti-G_h (purple) traces recorded at D and S. Right, Effects of anti-G_h on apparent R_{in}, sag, and RMP ($n = 5$). ***B***, Dendritic anti-G_h produced E-S potentiation. Firing probability versus EPSP slope in control (black) and with dendritic anti-G_h (purple) is shown. ***C***, Summary of the effects of dendritic anti-G_h on E-S coupling. ***D***, Recording configuration to test input specific facilitation in synaptic integration induced by injection of anti-G_h in the dendrite of a CA1 pyramidal neuron. ***E***, Normalized EPSP integral for each input when anti-G_h was injected. The change in the control input (St1) was always smaller than in the test input (St2). Hyperpol. Ampl., Hyperpolarization amplitude. *$p < 0.05$.

μM) (Chevaleyre and Castillo, 2002). Finally, the decay of extracellular and intracellular EPSP waveforms was equally affected after LTP induction and pharmacological blockade of I_h. Extracellular and intracellular EPSPs were slightly prolonged after LTP (Hess and Gustafsson, 1990; Asztely and Gustafsson, 1994).

Although our results support the fact that the downregulation of I_h represents a major mechanism accounting for enhanced dendritic integration in CA1 neurons, other mechanisms might be implicated. For instance, CA1 LTP is associated with a shift in the inactivation curve of dendritic A-type K^+ current toward hyperpolarizing values, thus reducing the impact of the A-current (Frick et al., 2004) (see also Losonczy et al., 2008). The downregulation of I_A could participate to E-S potentiation because pharmacological blockade of A-type K^+ channels facilitates EPSP amplitude (Hoffman et al., 1997) and enhances the amplitude–slope relationship of the EPSP (Campanac and Debanne, 2008). Furthermore, consistent with the input specificity of E-S potentiation, the changes in I_A are spatially restricted to a portion of dendrite in CA1 pyramidal neurons (Frick et al., 2004; Kim et al., 2007; Thompson, 2007; Losonczy et al., 2008). Alternatively, the activation curve of voltage-gated Na^+ channels is facilitated after LTP induction (Xu et al., 2005). In conclusion, the downregulation of I_h activity might be associated with the regulation of other conductances that will all facilitate dendritic integration.

Local reduction of I_h in the dendrites facilitates dendritic integration

Our data support the fact that the downregulation of I_h is restricted to a small dendritic region. The changes in G_h were relatively limited in amplitude. In contrast with the large hyperpolarizing shift observed when h-channel activity was globally reduced, the RMP at the soma remained largely unchanged after HFS. Injection of an anti-G_h in the dendrite differentially affected the RMP in the dendrite and the cell body. In L5 pyramidal neurons, the density of h-channels at distal dendritic sites may reach levels as high as 200–500 channels/μm^2 (Kole et al., 2006). Thus, given the anti-conductance used here (1–2.5 nS) and the unitary conductance of h-channels (0.68 pS), E-S potentiation could be the result of the functional downregulation of h-channels covering a dendritic area of $\sim$10–20 μm^2.

Long-term enhancement of dendritic integration associated with LTP is input specific (Daoudal et al., 2002; Wang et al., 2003; Xu et al., 2006; Campanac and Debanne, 2008). The injection of an anti-G_h in the apical dendrite at 50–100 μm from the soma mimicked this effect. In fact, integration of the synaptic input located near the site of anti-G_h injection was enhanced, whereas the integration of another input located closer to the soma remained largely unaffected. Our experimental results are compatible with mathematical models of synaptic integration in active dendrites. E-S potentiation simulated by adding local hot spots of depolarizing conductances in dendrites tends to be specific if the untetanized contacts are electrically closer to the soma than the tetanized contacts or if they are segregated to different primary dendrites (Wathey et al., 1992). Thus, input specific changes in dendritic integration are possible if I_h is locally reduced in the dendrites.

I_h may control dendritic integration via regulation of RMP. Global blockade of I_h induced a large hyperpolarization that produced E-S depression. More specifically, local electronic suppres-

sion of G_h in the dendrite affected RMP in the dendrite more than in the soma. This local hyperpolarization might affect the gating of many dendritic channels that shape the EPSP, thus altering integration. For instance, it may favor the recovery from inactivation of A-type K^+ channels, a major channel type in dendrites (Hoffman et al., 1997). In addition, the slight hyperpolarization might also decrease EPSP amplification mediated by Na^+ channels (Lipowsky et al., 1996). This hypothesis will require further studies, but it is reasonable to believe that these two effects may attenuate integration of neighboring inputs. Thus, the downregulation of I_h is compatible with the homosynaptic E-S potentiation and heterosynaptic E-S depression observed simultaneously after LTP induction (Daoudal et al., 2002).

E-S coupling is a complex operation in which any modification in EPSP waveform or spike threshold could produce a significant change. Although I_h determines EPSP amplitude and duration, its role in EPSP slope or spike threshold is negligible (Williams et al., 2007). Because the time constant of I_h is more than one order of magnitude slower than the EPSP rise time (~50 vs 2–3 ms), I_h blockers have no effect on EPSP-slope during the first 2 ms. For the same reasons, the AP threshold was virtually unaffected by ZD-7288. Thus, regulation of h-channels controls E-S coupling through the control of EPSP amplitude and decay.

Mechanisms for downregulation of I_h

The homeostatic upregulation of I_h requires NMDAR activation (Fan et al., 2005). Interestingly, the Hebbian downregulation of I_h also depends on activation of NMDARs permeable to Ca^{2+} ions. Thus, induction of both types of I_h regulations requires postsynaptic Ca^{2+} influx. The transition from Hebbian to homeostatic changes might be caused by increment in $[Ca^{2+}]$ recruiting different Ca^{2+} sensors. This kind of scenario has already been implicated in the transition from LTD to LTP (Lisman, 1989), but further studies will be required to identify the signaling pathways. Ca^{2+}-dependent protein kinases could be involved in linking Ca^{2+} transients to a persistent modification in I_h. One may speculate that the postsynaptic Ca^{2+} influx mediated by NMDAR may lead to the downregulation of I_h via activation of protein kinase C (PKC). Acute downregulation of I_h induced by neuromodulators (Cathala and Paupardin-Tritsch, 1997) and the facilitation in EPSP summation associated with LTP are mediated by PKC (Wang et al., 2003). Calcium/calmodulin kinase II (CaMKII) could also be involved (Fan et al., 2005), although the effects of CaMKII on h-channel activity remain unknown. Other mechanisms could be envisaged, because BDNF factor (brain-derived neurotrophic), proposed as a key actor in LTP, downregulates I_h in respiratory neurons (Thoby-Brisson et al., 2003). This mechanism is relatively unlikely here, because it implies a shift in the activation curve of the h-current. Although there has not been any study directly testing activity-dependent trafficking of hyperpolarization-activated cyclic nucleotide-gated cationic channel (HCN) subunits in neuronal plasticity, surface expression of I_h has been shown to be regulated through protein–protein interaction at the HCN C terminus by TRIP8b, a Rab-interacting brain-specific protein involved in vesicle trafficking (Santoro et al., 2004). Further investigation will be required to circumscribe the cellular and molecular mechanisms of dendritic h-channel regulation.

References

Abraham WC, Gustafsson B, Wigström H (1987) Long-term potentiation involves enhanced excitation relative to synaptic inhibition in guinea-pig hippocampus. J Physiol 394:367–380.

Abraham WC, Logan B, Greenwood JM, Dragunow M (2002) Induction and experience-dependent consolidation of stable long-term potentiation lasting months in the hippocampus. J Neurosci 22:9626–9634.

Andersen P (1990) Synaptic integration in hippocampal CA1 pyramids. Prog Brain Res 83:215–222.

Andersen P, Sundberg SH, Sveen O, Swann JW, Wigström H (1980) Possible mechanisms for long-lasting potentiation of synaptic transmission in hippocampal slices from guinea-pigs. J Physiol 302:463–482.

Asztely F, Gustafsson B (1994) Dissociation between long-term potentiation and associated changes in field EPSP waveform in the hippocampal CA1 region: an in vitro study in guinea pig brain slices. Hippocampus 4:148–156.

Bliss TV, Lømo T (1973) Long-lasting potentiation of synaptic transmission in the dentate area of the anaesthetized rabbit following stimulation of the perforant path. J Physiol 232:331–356.

Bliss TV, Lømo T, Gardner-Medwin AR (1973) Synaptic plasticity in the hippocampus. In: Macromolecules and Behaviour (Ansell G, Bradley PB, eds), pp 193–203. London: MacMillan.

Campanac E, Debanne D (2008) Spike timing-dependent plasticity: a learning rule for dendritic integration in rat CA1 pyramidal neurons. J Physiol 586:779–793.

Carlier E, Sourdet V, Boudkkazi S, Déglise P, Ankri N, Fronzaroli-Molinieres L, Debanne D (2006) Metabotropic glutamate receptor subtype 1 regulates sodium currents in rat neocortical pyramidal neurons. J Physiol 577:141–154.

Cathala L, Paupardin-Tritsch D (1997) Neurotensin inhibition of the hyperpolarization-activated cation current (I_h) in the rat substantia nigra pars compacta implicates the protein kinase C pathway. J Physiol 503:87–97.

Chen K, Aradi I, Thon N, Eghbal-Ahmadi M, Baram TZ, Soltesz I (2001) Persistently modified h-channels after complex febrile seizures convert the seizure-induced enhancement of inhibition to hyperexcitability. Nat Med 7:331–337.

Chevaleyre V, Castillo PE (2002) Assessing the role of Ih channels in synaptic transmission and mossy fiber LTP. Proc Natl Acad Sci U S A 99:9538–9543.

Daoudal G, Debanne D (2003) Long-term plasticity of intrinsic excitability: learning rules and mechanisms. Learn Mem 10:456–465.

Daoudal G, Hanada Y, Debanne D (2002) Bidirectional plasticity of excitatory postsynaptic potential (EPSP)-spike coupling in CA1 hippocampal pyramidal neurons. Proc Natl Acad Sci U S A 99:14512–14517.

Day M, Carr DB, Ulrich S, Ilijic E, Tkatch T, Surmeier DJ (2005) Dendritic excitability of mouse frontal cortex pyramidal neurons is shaped by the interaction among HCN, Kir2, and K_{leak} channels. J Neurosci 21:8776–8787.

Debanne D, Gähwiler BH, Thompson SM (1998) Long-term synaptic plasticity between pairs of individual CA3 pyramidal cells in rat hippocampal slice cultures. J Physiol 507:237–247.

Debanne D, Daoudal G, Sourdet V, Russier M (2003) Brain plasticity and ion channels. J Physiol Paris 97:403–414.

Fagni L, Zinebi F, Hugon M (1987) Evoked potential changes in rat hippocampal slices under helium pressure. Exp Brain Res 65:513–519.

Fan Y, Fricker D, Brager DH, Chen X, Lu HC, Chitwood RA, Johnston D (2005) Activity-dependent decrease of excitability in rat hippocampal neurons through increases in I_h. Nat Neurosci 8:1542–1551.

Frick A, Magee J, Johnston D (2004) LTP is accompanied by an enhanced local excitability of pyramidal neuron dendrites. Nat Neurosci 7:126–135.

Gasparini S, DiFrancesco D (1997) Action of the hyperpolarization-activated current (Ih) blocker ZD7288 in hippocampal CA1 neurons. Pflugers Arch 435:99–106.

Hanse E (2008) Associating synaptic and intrinsic plasticity. J Physiol 586:691–692.

Hess G, Gustafsson B (1990) Changes in field excitatory postsynaptic potential shape induced by tetanization in the CA1 region of the guinea-pig hippocampus. Neuroscience 37:61–69.

Hoffman DA, Magee JC, Colbert CM, Johnston D (1997) K+ channel regulation of signal propagation in dendrites of hippocampal pyramidal neurons. Nature 387:869–875.

Kim J, Jung SC, Clemens AM, Petralia RS, Hoffman DA (2007) Regulation of dendritic excitability by activity-dependant trafficking of the A-type K+ channel subunit Kv4.2 in hippocampal neurons. Neuron 54:933–947.

Kole MHP, Hallermann S, Stuart GJ (2006) Single I_h channels in pyramidal

neuron dendrites: properties, distribution, and impact on action potential output. J Neurosci 26:1677–1687.

Lipowsky R, Gillessen T, Alzheimer C (1996) Dendritic Na^+ channels amplify EPSPs in hippocampal CA1 pyramidal cells. J Neurophysiol 76:2181–2191.

Lisman J (1989) A mechanism for the Hebb and anti-Hebb processes underlying learning and memory. Proc Natl Acad Sci U S A 86:9574–9578.

Lörincz A, Notomi T, Tamás G, Shigemoto R, Nusser Z (2002) Polarized and compartment-dependent distribution of HCN1 in pyramidal cell dendrites. Nat Neurosci 5:1185–1193.

Losonczy A, Makara JK, Magee JC (2008) Compartmentalized dendritic plasticity and input feature storage in neurons. Nature 452:436–441.

Maccaferri G, Mangoni M, Lazzari A, DiFrancesco D (1993) Properties of the hyperpolarization-activated current in rat hippocampal CA1 pyramidal cells. J Neurophysiol 69:2129–2136.

Magee JC (1998) Dendritic hyperpolarization-activated currents modify the integrative properties of hippocampal CA1 pyramidal neurons. J Neurosci 18:7613–7624.

Marder CP, Buonomano DV (2003) Differential effects of short- and long-term potentiation on cell firing in the CA1 region of the hippocampus. J Neurosci 23:112–121.

Poolos NP, Migliore M, Johnston D (2002) Pharmacological upregulation of h-channels reduces the excitability of pyramidal neuron dendrites. Nat Neurosci 5:767–774.

Prinz AA, Abbott LF, Marder E (2004) The dynamic clamp comes of age. Trends Neurosci 27:218–224.

Reyes A (2001) Influence of dendritic conductances on the input-output properties of neurons. Annu Rev Neurosci 24:653–675.

Santoro B, Wainger BJ, Siegelbaum SA (2004) Regulation of HCN channel surface expression by a novel C-terminal protein–protein interaction. J Neurosci 24:10750–10762.

Spruston N (2008) Pyramidal neurons: dendritic structure and synaptic integration. Nat Rev Neurosci 9:206–221.

Spruston N, Jaffe DB, Johnston D (1994) Dendritic attenuation of synaptic potentials and currents: the role of passive membrane properties. Trends Neurosci 17:161–166.

Staff NP, Spruston N (2003) Intracellular correlate of EPSP-spike potentiation in CA1 pyramidal neurons is controlled by GABAergic modulation. Hippocampus 13:801–805.

Thoby-Brisson M, Cauli B, Champagnat J, Fortin G, Katz DM (2003) Expression of functional tyrosine kinase B receptors by rhythmically active respiratory neurons in the pre-Bötzinger complex of neonatal mice. J Neurosci 23:7685–7689.

Thompson SM (2007) I_A in play. Neuron 54:850–852.

Turrigiano GG, Nelson SB (2004) Homeostatic plasticity in the developing nervous system. Nat Rev Neurosci 5:97–107.

van Welie I, van Hooft JA, Wadman WJ (2004) Homeostatic scaling of neuronal excitability by synaptic modulation of somatic hyperpolarization-activated I_h channels. Proc Natl Acad Sci U S A 101:5123–5128.

Vasilyev DV, Barish ME (2002) Postnatal development of the hyperpolarization-activated excitatory current I_h in mouse hippocampal pyramidal neurons. J Neurosci 22:8992–9004.

Wang Z, Xu NL, Wu CP, Duan S, Poo MM (2003) Bidirectional changes in spatial dendritic integration accompanying long-term synaptic modifications. Neuron 37:463–472.

Wathey JC, Lytton WW, Jester JM, Sejnowski TJ (1992) Computer simulations of EPSP-spike (E-S) potentiation in hippocampal CA1 pyramidal cells. J Neurosci 12:607–618.

Williams SR, Wozny C, Mitchell SJ (2007) The back and forth of dendritic plasticity. Neuron 56:947–953.

Xu J, Kang N, Jiang L, Nedergaard M, Kang J (2005) Activity-dependent long-term potentiation of intrinsic excitability in hippocampal CA1 pyramidal neurons. J Neurosci 25:1750–1760.

Xu NL, Ye CQ, Poo MM, Zhang XH (2006) Coincidence detection of synaptic inputs is facilitated at the distal dendrites after long-term potentiation induction. J Neurosci 26:3002–3009.

Zhang W, Linden DJ (2003) The other side of the engram: experience-driven changes in neuronal intrinsic excitability. Nat Rev Neurosci 4:885–900.